ACS ES&T Engineering

pubs.acs.org/estengg

Article

Polarity Modulation Enhances Electrocatalytic Reduction of Nitrate by Iron Nanocatalysts

Yuren Feng, Xiaochuan Huang, Zhen-yu Wu, Haotian Wang, Kuichang Zuo,* and Qilin Li*

Cite This: https://doi.org/10.1021/acsestengg.3c00507

Read Online

ACCESS | Metrics & More | Article Recommendations | Supporting Information

ABSTRACT: Electrocatalytic reduction to convert nitrate (NO_3^-) to N_2 or NH_3 is of great interest for water and wastewater treatment, as well as N cycle management. However, the inherent electrostatic repulsion between the negatively charged nitrate ion and the cathode hinders nitrate adsorption on the catalyst and decreases reaction kinetics. In this study, we demonstrate that a simple polarity modulation strategy greatly enhances NO_3^- reduction catalyzed by an iron nanocatalyst immobilized on a carbon black electrode (Fe@CB). By switching between a positive and a negative potential, the system cycled through a short electrosorption step and a longer electrocatalytic reduction step. This increases the pseudo-first-order reaction rate constant of nitrate reduction from 2.46 to 3.09 h^{-1}, a 25.6% increase compared to the constant potential operation. The improved nitrate reduction kinetics was attributed to the enhanced nitrate adsorption during the electrosorption step, which improved the subsequent electrocatalytic reduction of NO_3^- upon reversal of the applied voltage. A short 30 s adsorption step at +0.1 V was found to enhance NO_3^- adsorption while avoiding reoxidation of reduced species formed in the previous reduction step. This operational strategy can be easily applied to other electrodes and catalysts, offering a simple, chemical-free, and cost-effective method for the removal of NO_3^- and valorization.

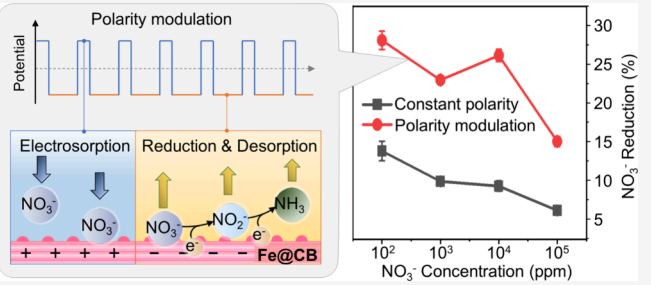

KEYWORDS: *nitrate, electrocatalytic reduction, polarity modulation, iron nanoparticle*

1. INTRODUCTION

Nitrate (NO_3^-) is a widespread containment in surface water and groundwater due to extensive fertilizer use and wastewater effluent discharge.[1−3] It is of great health concern due to its in vivo conversion to the toxic nitrite (NO_2^-) ion, excessive uptake of which can cause liver damage, blue baby symptoms, and cancer.[4,5,6] Although the drinking water standard for NO_3-N in the USA was set at 10 mg L^{-1} over 30 years ago,[7] NO_3^- remains the most frequently reported contaminant responsible for drinking water standard violations.[8] High NO_3^- concentrations up to 3000 mg of N/L have been reported worldwide in contaminated groundwater and wastewater.[9−13] Nitrate in surface water bodies can also cause eutrophication and lead to devastating algal bloom.[14] Therefore, removing NO_3^- from water and wastewater is of great significance for human and ecosystem health.

In recent years, there has been increasing interest in converting NO_3^- to ammonia (NH_3), a widely used fertilizer precursor, chemical feedstock, and fuel.[15−17] This is largely driven by the very high CO_2 emission of the current NH_3 production method[18] and the high demand for NH_3 for its traditional applications as well as its potential as a hydrogen carrier. Transforming the toxic NO_3^- in water and wastewater to NH_3 therefore represents a highly attractive waste-to-resource strategy.

Several existing technologies can effectively remove NO_3^- from water, including biological denitrification, adsorption, ion exchange, and reverse osmosis (RO). However, they each suffer from notable limitations. Biological denitrification can convert NO_3^- to innocuous binitrogen gas (N_2) but is slow in kinetics and highly sensitive to operating conditions such as temperature, pH, and carbon sources.[19−21] Adsorption, ion exchange, and RO separate NO_3^- from water instead of degrading it, producing waste brines containing high concentrations of NO_3^- that require further disposal. Degradation of nitrate in concentrated brine is still necessary for proper disposal.

Electrocatalysis has received great attention recently because it can degrade contaminants using electricity without adding chemicals or generating waste brines.[22−24] Extensive research has been performed on the electrocatalytic reduction of NO_3^-. Noble metals, e.g., palladium, platinum, and gold, are the most commonly used catalysts,[25−28] because their highly occupied

Received: October 25, 2023
Revised: January 25, 2024
Accepted: January 26, 2024

d-orbitals and unclosed outermost electron shell structure provide high electrocatalytic activity as well as stability.[24] However, noble metal catalysts are expensive due to the high cost of the precursors and the complex synthesis processes involved. Zero valent iron (ZVI) is a low-cost and abundant catalyst that has been shown to effectively reduce nitrate to produce ammonia. Several literatures have reported significant nitrate reduction and ammonia production using ZVI.[23,29,30] ZVI is commonly incorporated onto carbon substrates, e.g., activated carbon, graphene oxide, and carbon black (CB), by postsynthesis coating[31] or in situ reduction methods.[32,33] The substrate contributes to the electrocatalytic reaction by providing target contaminant adsorption sites in its porous structure, and thus enhancing reaction kinetics,[34,35] and/or improving electrical conductivity to lower energy consumption.[36,37]

It has been well established that NO_3^- adsorption onto the catalyst surface is essential to initiate the reduction of NO_3^- to NO_2^-, the first and rate-limiting step in reductive nitrate degradation.[24,38,39] Accordingly, significant effort has been made to enhance NO_3^- adsorption by increasing the electrode specific surface area or enhancing the NO_3^- mass transfer from the bulk solution to the electrode surface. In particular, flow-through electrodes in the form of packed bed reactors[40,41] and 3D porous monoliths,[42,43] which enable advective instead of diffusive transport of nitrate, have been shown to greatly improve NO_3^- reduction kinetics. However, the electric repulsion between the negatively charged NO_3^- ion and the catalysts on the cathode remains a significant hindrance to NO_3^- adsorption.[24,38,39,44,45]

In this study, we developed a simple polarity modulation technique that uses a low positive electric potential to induce the electrosorption of NO_3^- before a negative potential is applied for NO_3^- reduction. Using a CB electrode decorated with zerovalent iron nanoparticles as the catalyst, the polarity modulation method was evaluated and optimized for NO_3^- reduction over a wide range of initial NO_3^- concentrations. Relevant reaction mechanisms and long-term operation stability were elucidated.

2. MATERIALS AND METHODS

2.1. Chemicals and Materials. ELFTEX P100 CB powder was purchased from Cabot (USA). Ferric chloride ($FeCl_3$, 99%), sodium citrate dihydrate ($C_6H_9Na_3O_9$, 99%), sodium hydroxide (NaOH, 98.6%), sodium nitrate ($NaNO_3$, 99.7%), and sodium sulfate (Na_2SO_4, 99%) were purchased from Fisher Chemical (USA). Sulfanilamide ($C_6H_8N_2O_2S$, 98%), sodium nitroferricyanide dihydrate ($C_5FeN_6Na_2O\cdot_2H_2O$, 99%), and salicylic acid ($C_7H_6O_3$, 99%) were obtained from Acros Organics (USA). Sodium hypochlorite (NaClO, 5%) was obtained from LabChem (USA). Nafion-perfluorinated resin solution (5 wt %) was purchased from Sigma-Aldrich (USA). A glassy carbon plate was purchased from Yidian Technology (Shanghai, China); the Ag/AgCl reference electrode and Pt rod electrode were ordered from CH Instruments, Inc. (CHI660E, China). The Nafion 211 ion exchange membrane was obtained from Fuel Cell Earth (USA). All calibration standards were purchased from Fisher Scientific (USA) and used as received. All solutions were prepared in deionized (DI) water produced by a Barnstead E-Pure system (USA) with a resistivity of 18.2 MΩ cm^{-1}.

2.2. Electrode Preparation and Characterization. The nanozerovalent iron (NZVI) catalyst was loaded on CB particles by *in situ* NZVI formation. Briefly, 0.145 g of ferric chloride was mixed with 150 mL of DI water and sonicated for 2 h. The solution was mixed with 0.95 g of CB powder, sonicated for 0.5 h, and magnetically stirred overnight. The mixture was heated at 85 °C for 3 h in a rotary evaporator at a rotation speed of 50 rpm to dry. The solids were then harvested and ground into fine powder. Finally, the powder was heated at 600 °C in a tube furnace for 2 h in 5% H_2 in N_2 (UN1954, Airgas) to reduce the ferric species loaded on CB to NZVI.

To prepare electrodes, 10 mg of NZVI-loaded CB or pristine CB was mixed with 10 mL of isopropanol alcohol and 200 μL of 5 wt % Nafion solution and sonicated for at least 2 h. Then, 200 μL of the resulting suspension was applied to a 10 mm × 20 mm × 1 mm glassy carbon (GC) plate and vacuum-dried. The electrodes prepared using NZVI-loaded CB were referred to as Fe@CB electrodes. All electrodes were stored in a vacuum desiccator until use.

The surface morphology and composition of NZVI-loaded CB powder were characterized by scanning electron microscopy (SEM) using a Helios 660 SEM/FIB (USA). The fine structure and elemental mapping of NZVI-loaded CB were characterized by transmission electron microscopy (TEM) and high-angle annular dark-field TEM (HAADF-TEM) using an FEI Titan Themis[3] scanning/transmission electron microscopy (S/TEM) equipped with an energy-dispersive detector. The TEM was operated under an acceleration voltage of 300 kV. TEM samples were prepared by depositing a drop of an NZVI-loaded CB suspension on a carbon film-coated copper grid. X-ray diffraction of NZVI-loaded CB powder was performed using a Rigaku D/Max Ultima II Powder X-ray diffractometer with Cu Kα radiation, operated at 40 kV and 40 mA, and recorded from 0 to 60° (in 2θ). Cyclic voltammetry (CV) tests for the Fe@CB electrode were performed using a CHI 660E electrochemical workstation in a Na_2SO_4 solution with or without $NaNO_3$. The Na_2SO_4 concentration was 250 mmol L^{-1} in the absence of $NaNO_3$ and 100 mmol L^{-1} in the presence of 450 mmol L^{-1} $NaNO_3$ to maintain a constant total ionic strength of 750 mmol L^{-1}. During a CV test, the applied potential ranged from −1.0 to −1.8 V vs ACE with a scan rate of 10 mV s^{-1}.

2.3. Electrochemical Reduction of Nitrate. Electrochemical nitrate reduction experiments were conducted in a dual-chamber H cell equipped with three electrodes and a gas collector. As shown in Figure 1, the H cell was separated into two chambers by a Nafion 211 cation exchange membrane. The volume of each chamber is 30 mL. The Fe@CB electrode was used as the working electrode, a Pt wire was the counter electrode, and a Ag/AgCl electrode was used as the reference electrode. The working electrode and the reference electrode were installed in the same chamber to minimize the solution resistance. The gas collector was installed on the chamber that hosts the working and reference electrodes to collect and measure the volume of gases produced using the drainage gas collection method.[46] The reactor was completely sealed to be airtight.

In all nitrate reduction experiments, both the catholyte and anolyte chambers were first filled with 25 mL of $NaNO_3$ solution and the reactor was purged with argon gas for 10 min to remove oxygen before sealed. Experiments were performed in either a constant potential mode or a modulated polarity

https://doi.org/10.1021/acsestengg.3c00507
ACS EST Engg. XXXX, XXX, XXX−XXX

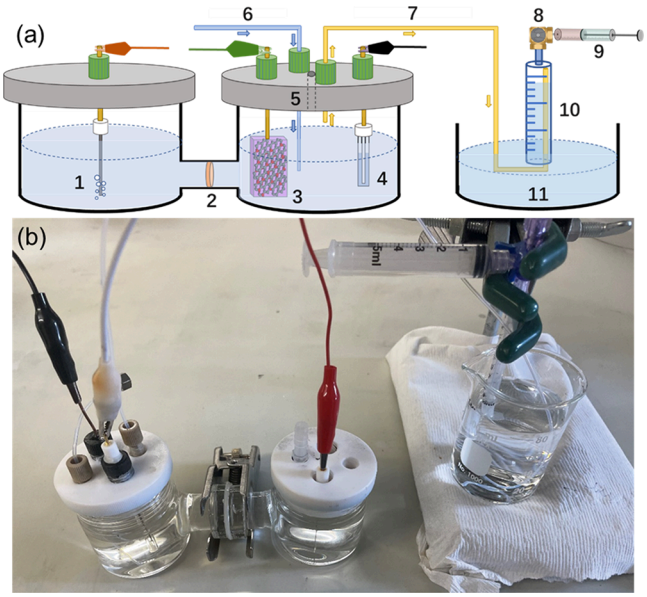

Figure 1. Schematic (a) and photograph (b) of the experimental system. 1: Pt counter electrode; 2: cation exchange membrane; 3: working electrode; 4: Ag/AgCl reference electrode; 5: sampling port; 6: argon inlet tube; 7: gas outlet tube; 8: two-way valve; 9: vacuuming syringe; 10: gas collecting syringe; 11: water container.

mode, with the applied potential provided by an electrochemical workstation (CHI660E, CH Instruments, China). In the constant potential operation mode, the cathodic potential was set constant at −0.7 V vs reverse hydrogen electrode (RHE), a potential that has been reported to initiate ammonia production.[47−49] In the polarity modulation mode, a cyclic electric potential pattern was applied. Each cycle consists of a short electrosorption phase, when a low positive potential of +0.1 V vs RHE is applied, and an electroreduction phase, when a potential of −0.7 V vs RHE was applied. The low positive potential, +0.1 V vs RHE, was chosen to induce electrosorption while minimizing potential reoxidation of reduced nitrogen species (as discussed later) as well as energy consumption. All electrical potential values reported were measured with respect to the Ag/AgCl reference electrode and converted to that versus RHE.[50] Current was recorded at 0.02 s intervals. All nitrate reduction experiments were repeated three times, using a freshly prepared electrode for each replicate experiment.

An initial nitrate concentration of 150 mmol L^{-1} (2100 mg of N/L) was used in most experiments, which represents the high nitrate concentrations found in some heavily contaminated water and wastewater.[9−13] Additional experiments were conducted at initial nitrate concentrations from 1.61 to 808 mmol L^{-1} (100−50,000 mg of NO_3^- L^{-1} or 22.58−11,290 mg of N L^{-1}) to study the impact of the initial nitrate concentration. Samples were taken in predetermined intervals from the chamber where the working electrode is installed and analyzed for pH, nitrate, nitrite, and ammonia. The nitrate concentration was determined by ion chromatography (ICS, Dionex, USA), while nitrite and ammonia concentrations were determined by colorimetric methods using a UV−vis spectroscope (Shimadzu UV-2550, Japan). Nitrite analysis followed the EPA standard method 354.1, whereas ammonia analysis followed a previously established method.[51−53]

The gas samples collected were analyzed by gas chromatography (TRACE 1310). To determine the presence of nitrogen gas, ultrahigh-purity nitrogen (Airgas company) was used as the standard.

3. RESULTS AND DISCUSSION

3.1. Electrode and Electrode Material Characterization. Figure 2 shows the characteristics of the as-synthesized NZVI-loaded CB powder. The SEM images (Figure 2a and Figure S1) show particles of 22.4 ± 5.2 nm in size, similar to the CB particles, which have an average diameter of 20.6 ± 7.8 nm (Figure S1). TEM characterization

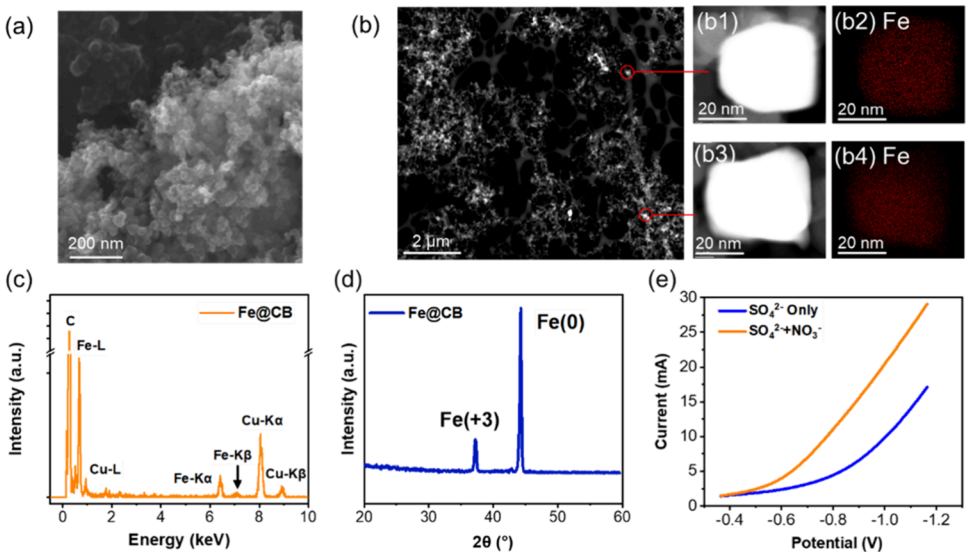

Figure 2. Characteristics of the NZVI-loaded CB powder and the Fe@CB electrode. (a) SEM and (B) TEM images of the NZVI-loaded CB. (b1, b3) High-angle annular dark-field (HAADF) TEM images showing strong signals from immobilized Fe nanoparticles; (b2, b4) EDS elemental mapping of Fe. (c) EDS spectrum of NZVI-loaded CB. The copper signal was from the lacey carbon copper-coated mesh; (d) XRD spectrum of NZVI-loaded CB. (e) Cyclic voltammetry curves of the Fe@CB electrode in a bisolute (100 mmol L^{-1} Na_2SO_4 + 450 mmol L^{-1} $NaNO_3$) solution and a single-solute (250 mmol L^{-1} Na_2SO_4) solution with the same total ionic strength of 750 mmol L^{-1}.

https://doi.org/10.1021/acsestengg.3c00507
ACS EST Engg. XXXX, XXX, XXX−XXX

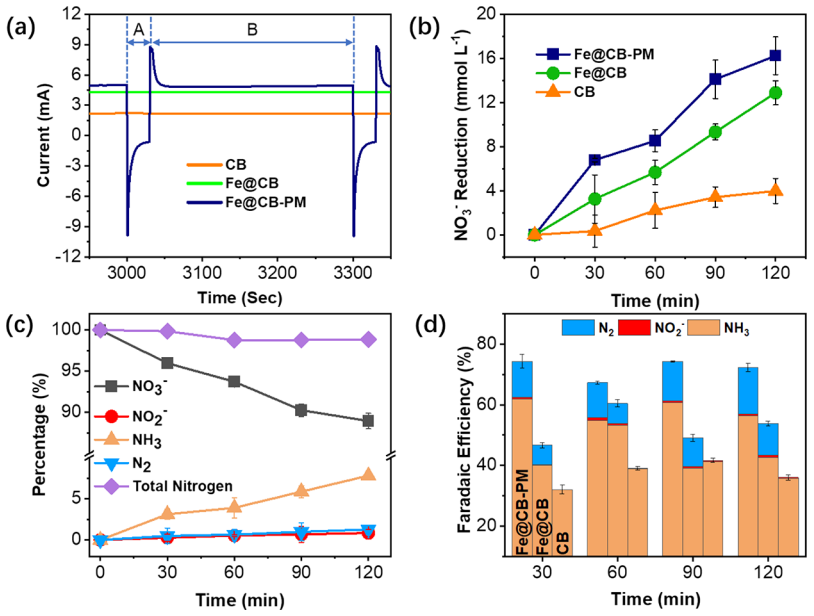

Figure 3. Electrochemical reduction of NO_3^- using the CB and Fe@CB electrodes. (a) Current production. A and B are the electrosorption and electrochemical reduction periods, respectively, in the polarity modulation mode (Fe@CB-PM). (b) The amount of NO_3^- reduced as a function of time. (c) Percentage of nitrogen species produced by the Fe@CB electrode with polarity modulation. (d) Faradaic efficiency of the CB and Fe@CB electrodes in different operation modes. CB: the CB electrode at a constant potential of −0.7 V. Fe@CB: the Fe@CB electrode at a constant potential of −0.7 V. Fe@CB-PM: the Fe@CB electrode with polarity modulation (cycles of 30 s at +0.1 V and 270 s at −0.7 V). Initial nitrate concentration: 150 mmol L^{-1}. Error bars represent the standard deviation from at least three replicate experiments.

(Figure 2b) found spots of high electron density, shown as strong signals with clear boundaries in the HAADF-STEM images (Figure 2b1,b3). These were identified as NZVI particles by EDS elemental mapping (Figure 2b2−b4). EDS analyses showed that the Fe mass loading was 44.4 mg g^{-1}, corresponding to a 0.98% atomic percentage (Figure 2c). XRD analyses found a large diffraction peak of zerovalent iron (Fe(0)) at 44.3°[54,55] and a small peak of Fe(III) at 37.3°[56,57] (Figure 2d). These results suggest that most Fe was successfully reduced to zero valence; a small amount of Fe^{3+} remained due to incomplete reduction or reoxidation of Fe(0). However, Fe^{3+} is assumed to not contribute significantly to the electrochemical nitrate reduction due to its higher redox potential than NO_3^-,[58] and the very small quantity present on the electrode.

CV tests showed the high reactivity of the Fe@CB electrode for NO_3^- reduction. As shown in Figure 2e, a current of 3.3 mA was observed at −0.7 V vs RHE in a 250 mmol L^{-1} Na_2SO_4 solution. As a comparison, the current more than doubled (7.5 mA) at the same potential in a solution containing 450 mmol L^{-1} $NaNO_3$ and 100 mmol L^{-1} Na_2SO_4, suggesting that the increase in the current was due to the occurrence of electrocatalytic nitrate reduction on the Fe@CB electrode.

3.2. Electrochemical Nitrate Reduction. To evaluate the electrochemical NO_3^- reduction performance in constant potential and polarity modulation modes, CB and Fe@CB electrodes were used to treat solutions containing 150 mmol L^{-1} NO_3^-. For the polarity modulation mode, the electrosorption phase lasted for 30 s and the electroreduction phase 270 s in each cycle; a total of 24 cycles were run in each polarity modulation experiment with a total reaction time of 2 h.

As shown in Figure S2 and Figure 3a, the CB electrode produced a positive and relatively stable current (2.3 ± 0.2 mA) when operated at a constant potential of −0.7 V. The current decreased slightly to 1.8 mA over a period of 60 min. As a comparison, the Fe@CB electrode operated at the same potential produced a notably higher current of 4.4 ± 0.1 mA, indicating that the Fe@CB electrode had a higher electrochemical catalytic activity than the CB electrode. When the potential of the Fe@CB electrode was modulated between +0.1 V (30 s per cycle) and −0.7 V (270 s per cycle), the current exhibited cyclic behavior accordingly: a negative current at +0.1 V and a positive current at −0.7 V. It is interesting to note that the steady-state current obtained in the electroreduction step (4.8 ± 0.2 mA) was higher than that obtained with a constant potential of −0.7 V (Figure 3a), indicating more electron transfer for nitrate reduction in the polarity modulation mode.

NO_3^- concentration data confirmed the catalytic activity of NZVI and the enhanced NO_3^- reduction kinetics with polarity modulation. As shown in Figure 3b, 3.98 mmol L^{-1} of NO_3^- was removed after 2 h of operation at a constant potential of −0.7 V using the CB electrode. Under the same conditions, the Fe@CB electrode achieved NO_3^- removal of 12.88 mmol L^{-1}, more than three times that obtained using the CB electrode; an even greater removal, 16.22 mmol L^{-1}, was obtained using the Fe@CB electrode when the polarity modulation mode was used, a 26% increase compared with that obtained in the constant potential mode. Similar enhancement was also observed using the CB electrode, as shown in Figure S3. These results show that polarity modulation enhances the electrochemical reduction of nitrate regardless of the electrode material used.

Consistent with previous studies,[24,59,60] electrochemical nitrate reduction using the CB electrode primarily generated NH_3 (eqs 1−3); 86.0% of NO_3^- reduced was transformed to NH_3 (Figure S4). A trace amount of NO_2^- (eq 1)[24] was also detected, but no N_2 production (eq 4) was detected. In

https://doi.org/10.1021/acsestengg.3c00507
ACS EST Engg. XXXX, XXX, XXX−XXX

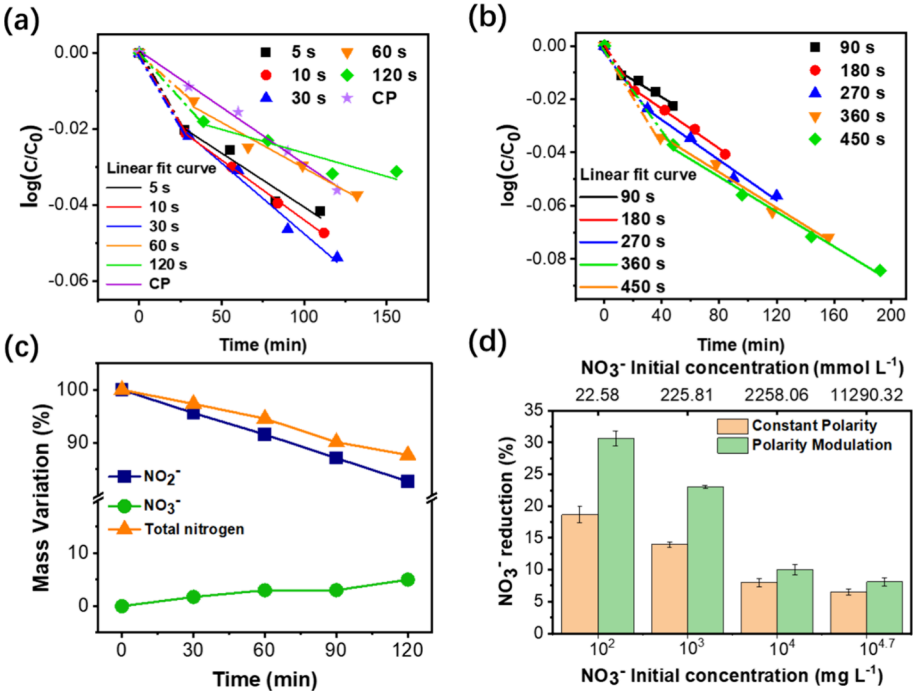

Figure 4. NO_3^- reduction kinetics in the polarity-modulated Fe@CB system with different (a) electrosorption times (reduction time fixed at 270 s) and (b) reduction times (electrosorption time fixed at 30 s). The solid lines represent linear regression with regression parameters listed in Tables S1 and S2, respectively. CP: constant potential. (c) Concentration of NO_2^-, NO_3^-, and their sum during a NO_2^- oxidation experiment. (d) NO_3^- reduction using the Fe@CB electrode at different initial NO_3^- concentrations. Error bars represent the standard deviation from at least three replicate experiments.

comparison, the Fe@CB electrode produced 19.5 μmol of N_2 in 2 h at a constant potential (Figure S4), which accounted for 12.1% of the total nitrate reduced (12.88 mmol L^{-1}, Figure 3b) and was much higher than that of the CB electrode. Because GC analyses of the gas collected found no other gases than N_2 (Figure S5), the amount of N_2 produced was calculated from the volume of the gas collected using the ideal gas law. 99.93% of the NH_3 produced is dissolved in the solution. The amount of NH_3 in the gas phase is nondetectable. The N_2 production of the Fe@CB electrode further increased to 26.2 μmol (accounting for 15.2% of the total nitrate reduced) in a 2 h experiment in the polarity modulation mode (Figure 3c). These results are consistent with previous studies,[61,62] which also reported N_2 production from NZVI.

Mass balance analyses revealed that a small amount of N was unaccounted for by the N species measured (Figure 3c). This may be attributed to the potential production of other intermediates (e.g., N_2O and NO) that were not measured.

During NO_3^- reduction, H^+ was consumed (eqs 1−4), leading to an increase in pH (Figure S6). The Fe@CB electrode with polarity modulation experienced the highest pH change (from 6.93 to 11.13), followed by Fe@CB (final pH of 10.85) and CB (final pH of 10.23) at a constant potential, corroborating the faster NO_3^- reduction kinetics of Fe@CB with polarity modulation.

$$NO_3^- + 2H^+ + 2e^- \rightarrow NO_2^- + H_2OE^0 = 0.\ 01\text{Vvs. SHE} \quad (1)$$

$$NO_2^- + H_2O + e^- \rightarrow NO + 2OH^-E^0 = -0.\ 47\text{Vvs. SHE} \quad (2)$$

$$NO + 5H^+ + 5e^- \rightarrow NH_3 + H_2OE^0 = 1.\ 06\text{Vvs. SHE} \quad (3)$$

$$2NO + 4H^+ + 4e^- \rightarrow N_2 + 2H_2OE^0 = 1.\ 77\text{Vvs. SHE} \quad (4)$$

Figure 3d compares the Faradaic efficiency calculated by eq 5 for nitrate reduction obtained by using the CB and Fe@CB electrodes:

$$\text{FE}(\%) = \frac{znF}{Q} = \frac{zCVF}{It} \times 100\% \quad (5)$$

Here, z is the number of electrons transferred; n is the number of moles of the product; F is the Faraday constant (96485 C mol^{-1}); Q is the total electric charge provided (C); C is the molar concentration of the product (mol L^{-1}); V is the solution volume (L); I is the current (A); and t is the reaction time (s). The highest overall Faradaic efficiency (67.3−74.3%) was obtained using the Fe@CB electrode with polarity modulation, followed by Fe@CB at a constant potential (46.7−60.5%) and the CB electrode at a constant potential (32.1−41.7%). The higher Faradaic efficiency of the Fe@CB compared to that of the CB electrode was attributed to the stronger NO_3^- binding to the NZVI due to electron donation from the highest occupied molecular orbital of NO_3^- to the empty orbital of Fe(0),[63] leading to suppression of the hydrogen evolution reaction (HER). The polarity modulation operation greatly improved the NO_3^- reduction Faradaic efficiency of the Fe@CB electrode, presumably due to enhanced adsorption of NO_3^- and other anions (e.g., NO_2^-) on the NZVI when a positive potential was applied (i.e., the electrosorption step). This is further discussed in the next section.

Similarly, the energy efficiency ratio (EER) was calculated by eq 6 to compare the amount of a reduction product generated

https://doi.org/10.1021/acsestengg.3c00507
ACS EST Engg. XXXX, XXX, XXX−XXX

per unit amount of energy consumption. The calculated EER values are listed in Figure S7.

$$\mathrm{EER}\left(\frac{\mathrm{mol}}{\mathrm{kWh}}\right) = \frac{n}{P} = \frac{C_p V}{UIt} \times 3.6 \times 10^6 \quad (6)$$

Here, P is the electricity consumed (kWh); U is the applied voltage (V); 3.6 × 106 is the joule-kWh converter; and C_p is the product concentration (mol L^{-1}). The EER for NH_3 production by the Fe@CB electrode in the polarity modulation mode is 45.76 mol/kWh, which is significantly higher than that obtained with a constant polarity (36.40 mol/kWh). The small positive potential applied in the electrosorption step generates low, nonfaradaic current and hence results in low energy use. This step, however, greatly enhances the Faradaic efficiency of the subsequent electroreduction step. Therefore, the overall energy consumption is greatly reduced. The CB electrode operated with a constant potential exhibited an EER of 29.32 mol/kWh for ammonia production; in the polarity modulation mode, the same CB electrode achieved an EER of 30.74 mol/kWh for ammonia production, a small increase from the constant potential mode.

3.3. Mechanism of Improved Nitrate Reduction on the Polarity-Modulated Fe@CB Electrode. In the polarity modulation mode, the electrosorption step improves nitrate reduction kinetics in the subsequent reduction step but also consumes electricity. Therefore, it is important to determine the effect of the duration of the electrosorption and reduction steps. To evaluate the effect of the electrosorption interval on the overall reduction kinetics, the duration of the reduction step was kept constant at 270 s in each cycle while that of the electrosorption step was varied between 5 and 120 s (Figure 4a and Figure S8). Data obtained under constant potential mode were also included for comparison.

As shown in Figure 4a, nitrate reduction by the Fe@CB electrode at a constant potential can be well described by a pseudo-first-order rate law with a rate constant of 2.46 h^{-1}, comparable with other electrodes reported in the literature (Table S1). Interestingly, the reaction kinetics in the polarity modulation mode exhibited two distinct phases; both can be described by a pseudo-first order rate law. A fast initial phase was followed by a slower phase, with rates in the second phase comparable to that obtained with a constant potential. The faster initial phase is attributed to the electrosorption of NO_3^- and hence the higher NO_3^- concentration on the NZVI for faster reduction reaction.

When the duration of the electrosorption phase increased, the overall nitrate reduction rate (r) first increased and then decreased, following the order of $r_{30s} > r_{10s} > r_{5s} > r_{CP} > r_{60s} > r_{120s}$, with the fastest nitrate reduction found at an electrosorption time of 30 s (Table S2). The increased reaction kinetics when the electrosorption time increased from 5 to 30 s is attributed to the increase in NO_3^- electrosorption; further increase in adsorption time, however, led to a decrease in NO_3^- reduction rate, which may be attributed to reoxidation of reduced N species. This is supported by the electrical current profile. As shown in Figure 3a, a sharp peak of a negative current occurred upon the onset of the electrosorption period due to the adsorption of NO_3^-. The current decreased quickly when the electrosorption approached equilibrium. However, it did not drop to zero, as typically observed in an electrosorption process. Instead, it stabilized at −0.5 mA after ∼30 s. This residual current, albeit small, suggests electron transfer to the anode, presumably from reduced N species generated in the previous reduction step, leading to their reoxidation.

To test this hypothesis, experiments were conducted using a 2 mmol L^{-1} $NaNO_2$ solution. Both chambers of the H cell were filled with a $NaNO_2$ solution. In the polarity modulation mode, the potential during the electrosorption step was kept at +0.1 V vs RHE whereas the applied potential during the electroreduction step changed to 0 V vs RHE to avoid reduction of NO_3^- that could potentially form from oxidation of NO_2^- during the electrosorption step. As shown in Figure 4c, the NO_3^- concentration in the solution increased while that of NO_2^- decreased with reaction time, showing that NO_2^- formed from NO_3^- reduction can be reoxidized in the subsequent electroadsorption step when a positive potential of +0.1 V is applied.

The same two-phase kinetics is also observed in Figure 4b, which shows the effect of electrochemical reduction time. In these experiments, the reduction time was varied between 90 and 450 s with the electrosorption time fixed at 30 s. When the duration of the electrochemical reduction step increased from 90 to 180 and 270 s, the pseudo-first-order rate constant in phase II increased from 2.68 to 3.09 and 3.13 h^{-1}, respectively (Figure S9 and Table S3). Further increases in the reduction step time, however, led to a decrease in the reaction rate constant. At a reduction step duration of 450 s, the pseudo-first order rate constant in phase II dropped to 2.71 h^{-1} (Table S3). This suggests that the reaction became mass transfer limited when the reduction time increased beyond 270 s. We hypothesized that with short reduction steps, the amount of NO_3^- adsorbed on the Fe@CB electrode during the electrosorption step was much more than what can be degraded during the reduction step, i.e., no mass transfer limitation; too long a reduction time, however, can exhaust the adsorbed NO_3^-, when additional nitrate reduction becomes mass transfer limited again.

The benefit of polarity modulation was found over a wide range of initial NO_3^- concentrations. Figure 4d compares NO_3^- reduction after 120 min reaction time at a constant potential (−0.7 V) and with polarity modulation (24 cycles of a 30 s electrosorption step followed by a 270 s reduction step). With initial NO_3^- concentrations ranging from 100 to 50,000 ppm, the polarity modulation operation achieved 24.1 to 64.2% more NO_3^- reduction compared with a constant potential. The enhancement of nitrate reduction by polarity modulation is more prominent at lower initial nitrate concentrations. At 100 mg/L initial nitrate concentration, the polarity modulation mode exhibited 64.2% more nitrate reduction than the constant potential mode while the difference was only 24.1% at 50,000 mg/L. This is consistent with the hypothesis that polarity modulation eliminates the mass transfer limitation as mass transfer is faster at higher bulk concentrations.

3.4. Long-Term Electrode Stability. Long-term stability of the electrode is an important factor determining the cost-effectiveness of the electrochemical treatment. In the polarity modulation mode, the application of the positive potential during the electrosorption phase, albeit short, may lead to the oxidation of metal catalysts and cause electrode corrosion over long-term operation.

To assess the stability of the Fe@CB electrode in the polarity modulation mode, a freshly prepared Fe@CB electrode was tested in 10 consecutive experiments, each run

https://doi.org/10.1021/acsestengg.3c00507
ACS EST Engg. XXXX, XXX, XXX−XXX

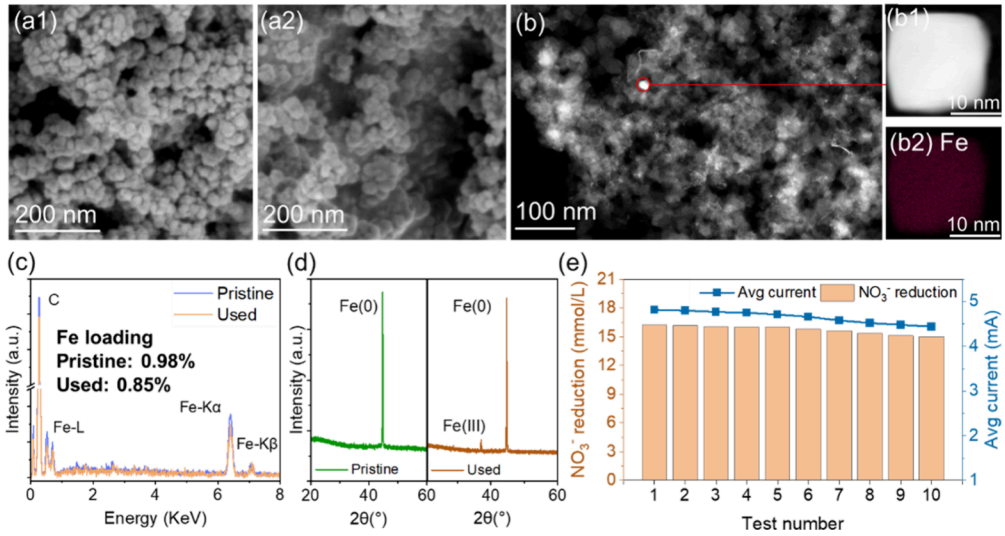

Figure 5. Characteristics and performance of the Fe@CB electrode during the long-term stability test. (a) SEM images of the Fe@CB electrode before (a1) and after the stability test (a2). (b) TEM image of the Fe@CB electrode. (b1) High-angle annular dark-field (HAADF) images showing strong signal from immobilized Fe nanoparticles; (b2) EDS elemental mapping of Fe; (c) EDS spectra of the pristine and used Fe@CB electrode; (d) XRD spectra of the pristine and used Fe@CB electrode; (e) NO_3^- reduction and average current during the reduction phase obtained in the 10 consecutive run. Avg: average.

for 2 h. The nitrate solution was replaced with a fresh one at the beginning of every experiment. The Fe@CB electrode was characterized before and after use.

After the stability test, the Fe@CB electrode exhibited no visible changes in its morphology, as shown in the SEM images (Figure 5a1,a2). The NZVI-loaded CB particles retained their spherical shape, and the particle average diameter (21.4 ± 4.6 nm) was similar to that of the freshly prepared catalysts (20.32 ± 6.6 nm) (Figure S10). TEM analyses found high electron density spots similar to those shown in Figure 2b, which were further identified by HAADF-STEM images and EDS elemental mapping (Figure 5b1,b2) as NZVI. However, EDS analysis (Figure 5c) of the electrode revealed a small loss of Fe: Fe loading decreased from 0.98 to 0.85% after the experiment. This is attributed to the oxidation of Fe(0) to Fe(III) during the electrosorption phase and the subsequent leaching of Fe(III). According to the Pourbaix diagram,[64] Fe(III) forms at +0.1 V at pH 3.7 to 14, the condition encountered in the electrosorption step. This was confirmed by XRD analyses as shown in Figure 5d. The Fe@CB electrode prepared for the long-term stability test was preserved in an anaerobic environment to prevent oxidation by air. XRD analyses of the freshly prepared catalyst found only one peak at 44.3°, suggesting that NZVI was the only Fe species on the electrode. However, a small Fe(III) peak appeared at 37.3° in the XRD spectrum of the electrode after the stability test, suggesting that 8.5% of Fe(0) was converted to Fe(III). The small amount of Fe oxidation is consistent with the low positive voltage and short time of the electrosorption step. Dissolution and leaching of Fe(III) are believed to be responsible for the small loss of Fe loading over time.

The loss of NZVI led to a small decline of the electrode performance over time of use, as shown in Figure 5e. Nitrate reduction decreased from 16.22 mmol/L in the first 2 h run to 15.02 mmol/L in the 10th 2 h experiment, a 7.4% decline in electrode performance. This is also consistent with the small decline in electric current from 4.8 to 4.4 mA.

4. CONCLUSIONS

The reported study demonstrates significant enhancement of electrochemical NO_3^- reduction kinetics by an Fe@CB electrode using a simple polarity modulation technique. In the polarity modulation mode, a short electrosorption step induced by a low positive potential overcomes the mass transfer limitation of NO_3^- adsorption, accelerating the subsequent electrocatalytic reduction of adsorbed NO_3^-, which also regenerates the adsorption sites. The synergy between electrosorption and electrocatalytic reduction generated in the cyclic operation enhanced NO_3^- supply on the NZVI surface and greatly improved Faradaic efficiency for NO_3^- reduction. This simple technique provides a low-pressure, low-voltage, high-energy-efficiency, and chemical-free method to treat water containing a wide range of NO_3^- concentrations. Compared to other methods that have been used to enhance nitrate reduction kinetics (e.g., flow-through electrodes), it does not require any changes in the electrode or reactor design and is simple to implement. The nonspecific interaction (i.e., electrostatic attraction) utilized in the electrosorption step also suggests that the polarity modulation approach can be applied to electrocatalytic reduction of other anions such as chromate,[65] selenate, and selenite. It is important, however, to note that the polarity modulation cycles need to be optimized for different contaminants and catalysts, as the optimal electrosorption and reduction intervals are a complex function of the adsorption kinetics as well as the redox reactions involved. The positive potential applied during the electrosorption step, both low and short, may lead to oxidation and subsequent leaching of the metal catalyst, which should also be carefully considered in process optimization.

■ ASSOCIATED CONTENT

Supporting Information

The Supporting Information is available free of charge at https://pubs.acs.org/doi/10.1021/acsestengg.3c00507.

Particle size distribution for carbon black particles; current production of the CB and Fe@CB electrodes at

https://doi.org/10.1021/acsestengg.3c00507
ACS EST Engg. XXXX, XXX, XXX−XXX

different experiment conditions; amount of NO_3^- reduced as a function of time using the carbon black (CB) electrode; the concentration of produced nitrogen species by Fe@CB and pristine CB electrode under both constant and modulated polarity condition in 2 h experiments; gas chromatography analysis of the gas sample collected from a 2 h Fe@CB electrode polarity modulation experiment; variation of pH for CB and Fe@CB electrodes at different experiment conditions; energy efficiency ratio (EER) for the CB and Fe@CB electrodes under constant polarity and polarity modulation modes; the amount of NO_3^- reduction and ammonia production with different adsorption time lengths; The amount of NO_3^- reduction and ammonia production with different reduction time lengths; particle size distribution for NZVI-loaded CB particles before and after the long-term stability test; kinetic studies in NO_3^- electrochemical reduction-related publications by different cathode materials; kinetic studies for nitrate reduction under different adsorption time lengths; and nitrate reduction kinetics under different reduction time lengths (PDF)

AUTHOR INFORMATION

Corresponding Authors

Kuichang Zuo − *The Key Laboratory of Water and Sediment Sciences, Ministry of Education; College of Environment Sciences and Engineering, Peking University, Beijing 100871, China;* orcid.org/0000-0002-3922-8702; Email: kuichang.zuo@pku.edu.cn

Qilin Li − *Department of Civil and Environmental Engineering, NSF Nanosystems Engineering Research Center Nanotechnology-Enabled Water Treatment, Department of Chemical and Biomolecular Engineering, and Department of Materials Science and Nanoengineering, Rice University, Houston, Texas 77005, United States;* orcid.org/0000-0001-5756-3873; Phone: (713) 348-2046; Email: qilin.li@rice.edu

Authors

Yuren Feng − *Department of Civil and Environmental Engineering and NSF Nanosystems Engineering Research Center Nanotechnology-Enabled Water Treatment, Rice University, Houston, Texas 77005, United States*

Xiaochuan Huang − *Department of Civil and Environmental Engineering and NSF Nanosystems Engineering Research Center Nanotechnology-Enabled Water Treatment, Rice University, Houston, Texas 77005, United States*

Zhen-yu Wu − *Department of Chemical and Biomolecular Engineering, Rice University, Houston, Texas 77005, United States*

Haotian Wang − *NSF Nanosystems Engineering Research Center Nanotechnology-Enabled Water Treatment and Department of Chemical and Biomolecular Engineering, Rice University, Houston, Texas 77005, United States;* orcid.org/0000-0002-3552-8978

Complete contact information is available at: https://pubs.acs.org/10.1021/acsestengg.3c00507

Notes

The authors declare that they have no known competing financial interests or personal relationships that could have appeared to influence the work reported in this paper.
The authors declare no competing financial interest.

ACKNOWLEDGMENTS

This project was supported by NSF Nanosystems Engineering Research Center for Nanotechnology-Enabled Water Treatment (EEC-1449500). We also gratefully acknowledge Shun Wang and Dr. Xinmin Zhan at National University of Ireland, Galway, who assisted with the design of the N_2 collection device. The authors also acknowledge Shared Equipment Authority at Rice University for access and utilization of characterization instrumentation and the use of Electron Microscopy Center (EMC) at Rice University.

REFERENCES

(1) Xie, Y.; Cao, H.; Li, Y.; Zhang, Y.; Crittenden, J. C. Highly Selective PdCu/Amorphous Silica−Alumina (ASA) Catalysts for Groundwater Denitration. *Environ. Sci. Technol.* **2011**, *45* (9), 4066−4072.

(2) Centi, G.; Perathoner, S. Remediation of Water Contamination Using Catalytic Technologies. *Applied Catalysis B: Environmental* **2003**, *41* (1), 15−29.

(3) Jeong, J.-Y.; Kim, H.-K.; Kim, J.-H.; Park, J.-Y. Electrochemical Removal of Nitrate Using ZVI Packed Bed Bipolar Electrolytic Cell. *Chemosphere* **2012**, *89* (2), 172−178.

(4) Spalding, R. F.; Exner, M. E. Occurrence of Nitrate in Groundwater—A Review. *Journal of Environmental Quality* **1993**, *22* (3), 392−402.

(5) Gupta, S. K.; Gupta, R. C.; Gupta, A. B.; Seth, A. K.; Bassin, J. K.; Gupta, A. Recurrent Acute Respiratory Tract Infections in Areas with High Nitrate Concentrations in Drinking Water. *Environ. Health Perspect* **2000**, *108* (4), 363−366.

(6) Majumdar, D.; Gupta, N. Nitrate Pollution of Groundwater and Associated Human Health Disorders. *Indian J. Environ. Health* **2000**, *42*, 28−39.

(7) EPA *Nitrate; CASRN 14797−55−8*; EPA, Series Ed.; 1991.

(8) Pennino, M. J.; Compton, J. E.; Leibowitz, S. G. Trends in Drinking Water Nitrate Violations Across the United States. *Environ. Sci. Technol.* **2017**, *51* (22), 13450−13460.

(9) Cyplik, P.; Marecik, R.; Piotrowska-Cyplik, A.; Olejnik, A.; Drożdżyńska, A.; Chrzanowski, Ł. Biological Denitrification of High Nitrate Processing Wastewaters from Explosives Production Plant. *Water Air Soil Pollut* **2012**, *223* (4), 1791−1800.

(10) Fernández-Nava, Y.; Marañón, E.; Soons, J.; Castrillón, L. Denitrification of Wastewater Containing High Nitrate and Calcium Concentrations. *Bioresour. Technol.* **2008**, *99* (17), 7976−7981.

(11) Fernández-Nava, Y.; Marañón, E.; Soons, J.; Castrillón, L. Denitrification of High Nitrate Concentration Wastewater Using Alternative Carbon Sources. *Journal of Hazardous Materials* **2010**, *173* (1), 682−688.

(12) Nugroho, R.; Ikbal; Said, N. I.; Hasanuddin. Denitrification of Ammonium Nitrate Industrial Wastewater Using Sulfur and Limestone Packed Bioreactor. *IOP Conf. Ser.: Earth Environ. Sci.* **2023**, *1201* (1), No. 012010.

(13) Pazhuparambil Jayarajan, S. K.; Kuriachan, L. Exposure and Health Risk Assessment of Nitrate Contamination in Groundwater in Coimbatore and Tirupur Districts in Tamil Nadu, South India. *Environ. Sci. Pollut Res. Int.* **2021**, *28* (8), 10248−10261.

(14) Smolders, A. J. P.; Lucassen, E. C. H. E. T.; Bobbink, R.; Roelofs, J. G. M.; Lamers, L. P. M. How Nitrate Leaching from Agricultural Lands Provokes Phosphate Eutrophication in Groundwater Fed Wetlands: The Sulphur Bridge. *Biogeochemistry* **2010**, *98* (1), 1−7.

(15) Lee, J.; Choi, Y.; Choi, J. Techno-Economic Analysis of NH3 Fuel Supply and Onboard Re-Liquefaction System for an NH3-Fueled Ocean-Going Large Container Ship. *Journal of Marine Science and Engineering* **2022**, *10* (10), 1500.
(16) Wang, Y.; Xu, A.; Wang, Z.; Huang, L.; Li, J.; Li, F.; Wicks, J.; Luo, M.; Nam, D.-H.; Tan, C.-S.; Ding, Y.; Wu, J.; Lum, Y.; Dinh, C.-T.; Sinton, D.; Zheng, G.; Sargent, E. H. Enhanced Nitrate-to-Ammonia Activity on Copper−Nickel Alloys via Tuning of Intermediate Adsorption. *J. Am. Chem. Soc.* **2020**, *142* (12), 5702−5708.
(17) Zhao, Z.; Zhang, Z.; Zha, X.; Gao, G.; Mao, W.; Wu, F.; Li, X.; Luo, C.; Zhang, L. Fuel-NO Formation Mechanism in MILD-Oxy Combustion of CH4/NH3 Fuel Blend. *Fuel* **2023**, *331*, No. 125817.
(18) Hirakawa, H.; Hashimoto, M.; Shiraishi, Y.; Hirai, T. Selective Nitrate-to-Ammonia Transformation on Surface Defects of Titanium Dioxide Photocatalysts. *ACS Catal.* **2017**, *7* (5), 3713−3720.
(19) Dawson, R. N.; Murphy, K. L. The Temperature Dependency of Biological Denitrification. *Water Res.* **1972**, *6* (1), 71−83.
(20) Ahmed, S. M.; Rind, S.; Rani, K. Systematic Review: External Carbon Source for Biological Denitrification for Wastewater. *Biotechnol. Bioeng.* **2023**, *120* (3), 642−658.
(21) Shrimali, M.; Singh, K. P. New Methods of Nitrate Removal from Water. *Environ. Pollut.* **2001**, *112* (3), 351−359.
(22) Bhatnagar, A.; Sillanpää, M. A Review of Emerging Adsorbents for Nitrate Removal from Water. *Chemical Engineering Journal* **2011**, *168* (2), 493−504.
(23) Della Rocca, C.; Belgiorno, V.; Meriç, S. Overview of In-Situ Applicable Nitrate Removal Processes. *Desalination* **2007**, *204* (1), 46−62.
(24) Garcia-Segura, S.; Lanzarini-Lopes, M.; Hristovski, K.; Westerhoff, P. Electrocatalytic Reduction of Nitrate: Fundamentals to Full-Scale Water Treatment Applications. *Applied Catalysis B: Environmental* **2018**, *236*, 546−568.
(25) Costa, A. O.; Ferreira, L. S.; Passos, F. B.; Maia, M. P.; Peixoto, F. C. Microkinetic Modeling of the Hydrogenation of Nitrate in Water on Pd−Sn/Al2O3 Catalyst. *Applied Catalysis A: General* **2012**, *445*−*446*, 26−34.
(26) El-Deab, M. S. Electrochemical Reduction of Nitrate to Ammonia at Modified Gold Electrodes. *Electrochim. Acta* **2004**, *49* (9), 1639−1645.
(27) Tsai, M.-C.; Zhuang, D.-X.; Chen, P.-Y. Electrodeposition of Macroporous Silver Films from Ionic Liquids and Assessment of These Films in the Electrocatalytic Reduction of Nitrate. *Electrochim. Acta* **2010**, *55* (3), 1019−1027.
(28) Yang, J.; Sebastian, P.; Duca, M.; Hoogenboom, T.; Koper, M. T. M. pH Dependence of the Electroreduction of Nitrate on Rh and Pt Polycrystalline Electrodes. *Chem. Commun.* **2014**, *50* (17), 2148−2151.
(29) Baek, K.; Kasem, N.; Ciblak, A.; Vesper, D.; Padilla, I.; Alshawabkeh, A. N. Electrochemical Removal of Selenate from Aqueous Solutions. *Chemical Engineering Journal* **2013**, *215*−*216*, 678−684.
(30) Xu, D.; Li, Y.; Yin, L.; Ji, Y.; Niu, J.; Yu, Y. Electrochemical Removal of Nitrate in Industrial Wastewater. *Front. Environ. Sci. Eng.* **2018**, *12* (1), 9.
(31) Pu, S. Y.; Deng, D. L.; Wang, K. X.; Wang, M. T.; Zhang, Y.; Shangguan, L. X.; Chu, W. Optimizing the Removal of Nitrate from Aqueous Solutions via Reduced Graphite Oxide-Supported NZVI: Synthesis, Characterization, Kinetics, and Reduction Mechanism. *Environmental Science and Pollution Research* **2019**, *26* (4), 3932−3945.
(32) Jiang, Q.; Zhang, Y.; Jiang, S.; Wang, Y.; Li, H.; Han, W.; Qu, J.; Wang, L.; Hu, Y. Graphene-like Carbon Sheet-Supported NZVI for Efficient Atrazine Oxidation Degradation by Persulfate Activation. *Chemical Engineering Journal* **2021**, *403*, No. 126309.
(33) Kao, C.-Y.; Chou, K.-S. Iron/Carbon-Black Composite Nanoparticles as an Iron Electrode Material in a Paste Type Rechargeable Alkaline Battery. *J. Power Sources* **2010**, *195* (8), 2399−2404.
(34) Ahmad, M.; Ahmad, M.; Usman, A. R. A.; Al-Faraj, A. S.; Abduljabbar, A. S.; Al-Wabel, M. I. Biochar Composites with Nano Zerovalent Iron and Eggshell Powder for Nitrate Removal from Aqueous Solution with Coexisting Chloride Ions. *Environ. Sci. Pollut Res.* **2018**, *25* (26), 25757−25771.
(35) Liu, G.; Zhou, Y.; Liu, Z.; Zhang, J.; Tang, B.; Yang, S.; Sun, C. Efficient Nitrate Removal Using Micro-Electrolysis with Zero Valent Iron/Activated Carbon Nanocomposite. *J. Chem. Technol. Biotechnol.* **2016**, *91* (12), 2942−2949.
(36) Pignatello, J. J.; Mitch, W. A.; Xu, W. Activity and Reactivity of Pyrogenic Carbonaceous Matter toward Organic Compounds. *Environ. Sci. Technol.* **2017**, *51* (16), 8893−8908.
(37) Wei, A.; Ma, J.; Chen, J.; Zhang, Y.; Song, J.; Yu, X. Enhanced Nitrate Removal and High Selectivity towards Dinitrogen for Groundwater Remediation Using Biochar-Supported Nano Zero-Valent Iron. *Chemical Engineering Journal* **2018**, *353*, 595−605.
(38) Zhang, X.; Wang, Y.; Liu, C.; Yu, Y.; Lu, S.; Zhang, B. Recent Advances in Non-Noble Metal Electrocatalysts for Nitrate Reduction. *Chemical Engineering Journal* **2021**, *403*, No. 126269.
(39) Wang, Y.; Wang, C.; Li, M.; Yu, Y.; Zhang, B. Nitrate Electroreduction: Mechanism Insight, in Situ Characterization, Performance Evaluation, and Challenges. *Chem. Soc. Rev.* **2021**, *50*, 6720−6733.
(40) Kim, H. K.; Jeong, J. Y.; Cho, H. N.; Park, J. Y. Kinetics of Nitrate Reduction with the Packed Bed Iron Bipolar Electrode. *Sep. Purif. Technol.* **2015**, *152*, 140−147.
(41) Ma, J.; Wei, W.; Qin, G.; Jiang, L.; Hing Wong, N.; Sunarso, J.; Liu, S. Integrated Electrocatalytic Packed-Bed Membrane Reactor for Nitrate Removal. *Sep. Purif. Technol.* **2022**, *292*, No. 121010.
(42) Mattarozzi, L.; Cattarin, S.; Comisso, N.; Gerbasi, R.; Guerriero, P.; Musiani, M.; Vazquez-Gomez, L.; Verlato, E. Electrodeposition of Cu-Ni Alloy Electrodes with Bimodal Porosity and Their Use for Nitrate Reduction. *ECS Electrochemistry Letters* **2013**, *2* (11), D58−D60.
(43) Cerrón-Calle, G. A.; Fajardo, A. S.; Sánchez-Sánchez, C. M.; Garcia-Segura, S. Highly Reactive Cu-Pt Bimetallic 3D-Electrocatalyst for Selective Nitrate Reduction to Ammonia. *Applied Catalysis B: Environmental* **2022**, *302*, No. 120844.
(44) de Groot, M. T.; Koper, M. T. M. The Influence of Nitrate Concentration and Acidity on the Electrocatalytic Reduction of Nitrate on Platinum. *J. Electroanal. Chem.* **2004**, *562* (1), 81−94.
(45) Dima, G. E.; Beltramo, G. L.; Koper, M. T. M. Nitrate Reduction on Single-Crystal Platinum Electrodes. *Electrochim. Acta* **2005**, *50* (21), 4318−4326.
(46) Roper, J. D.; Burton, D. L.; Madani, A.; Stratton, G. W. A Simple Method for Quantifying Dissolved Nitrous Oxide in Tile Drainage Water. *Can. J. Soil. Sci.* **2013**, *93* (1), 59−64.
(47) Fan, X.; Ma, C.; Zhao, D.; Deng, Z.; Zhang, L.; Wang, Y.; Luo, Y.; Zheng, D.; Li, T.; Zhang, J.; Sun, S.; Lu, Q.; Sun, X. Unveiling Selective Nitrate Reduction to Ammonia with Co3O4 Nanosheets/TiO2 Nanobelt Heterostructure Catalyst. *J. Colloid Interface Sci.* **2023**, *630*, 714−720.
(48) Lv, Y.; Su, J.; Gu, Y.; Tian, B.; Ma, J.; Zuo, J.-L.; Ding, M. Atomically Precise Integration of Multiple Functional Motifs in Catalytic Metal−Organic Frameworks for Highly Efficient Nitrate Electroreduction. *JACS Au* **2022**, *2* (12), 2765−2777.
(49) Wu, Z.-Y.; Karamad, M.; Yong, X.; Huang, Q.; Cullen, D. A.; Zhu, P.; Xia, C.; Xiao, Q.; Shakouri, M.; Chen, F.-Y.; Kim, J. Y. T.; Xia, Y.; Heck, K.; Hu, Y.; Wong, M. S.; Li, Q.; Gates, I.; Siahrostami, S.; Wang, H. Electrochemical Ammonia Synthesis via Nitrate Reduction on Fe Single Atom Catalyst. *Nat. Commun.* **2021**, *12* (1), 2870.
(50) Niu, S.; Li, S.; Du, Y.; Han, X.; Xu, P. How to Reliably Report the Overpotential of an Electrocatalyst. *ACS Energy Lett.* **2020**, *5* (4), 1083−1087.
(51) Duncan, A. B. F. The Ultraviolet Absorption Spectrum of Ammonia. *Phys. Rev.* **1935**, *47* (11), 822−827.

https://doi.org/10.1021/acsestengg.3c00507
ACS EST Engg. XXXX, XXX, XXX−XXX

(52) Wang, Y.; Yu, Y.; Jia, R.; Zhang, C.; Zhang, B. Electrochemical Synthesis of Nitric Acid from Air and Ammonia through Waste Utilization. *National Science Review* **2019**, *6* (4), 730−738.
(53) Zhu, D.; Zhang, L.; Ruther, R. E.; Hamers, R. J. Photo-Illuminated Diamond as a Solid-State Source of Solvated Electrons in Water for Nitrogen Reduction. *Nat. Mater.* **2013**, *12* (9), 836−841.
(54) Khorsandi, H.; Azarnioush, A.; Aghapour, A.; Nemati, S.; Karimzadeh, S.; Khalkhali, H. An Analysis of Boron Removal from Water Using Modified Zero-Valent Iron Nanoparticles. *DESALINATION AND WATER TREATMENT* **2017**, *70*, 284−289.
(55) Liang, W.; Dai, C.; Zhou, X.; Zhang, Y. Application of Zero-Valent Iron Nanoparticles for the Removal of Aqueous Zinc Ions under Various Experimental Conditions. *PLoS One* **2014**, *9* (1), No. e85686.
(56) Liu, T.; Shen, H.; Wang, C.; Chou, W. Structure Evolution of Y2O3 Nanoparticle/Fe Composite during Mechanical Milling and Annealing. *Progress in Natural Science: Materials International* **2013**, *23* (4), 434−439.
(57) Chen, D.; Chen, S.; Jiang, Y.; Xie, S.; Quan, H.; Hua, L.; Luo, X.; Guo, L. Heterogeneous Fenton-like Catalysis of Fe-MOF Derived Magnetic Carbon Nanocomposites for Degradation of 4-Nitrophenol. *RSC Adv.* **2017**, *7* (77), 49024−49030.
(58) Bard, A. J.; Faulkner, L. R.; White, H. S. Electrochemical Methods: Fundamentals and Applications, Wiley: New York, 2nd Ed. *Russ. J. Electrochem.* 2002, *38* (12), 1364−1365. DOI: 10.1023/A:1021637209564.
(59) Kuang, P.; Feng, C.; Chen, N.; Hu, W.; Wang, G.; Peng, T.; Lv, L. Improvement on Electrochemical Nitrate Removal by Combining with the Three-Dimensional (3-D) Perforated Iron Cathode and the Iron Net Introduction. *J. Electrochem. Soc.* **2016**, *163* (14), E397−E406.
(60) Tokazhanov, G.; Ramazanova, E.; Hamid, S.; Bae, S.; Lee, W. Advances in the Catalytic Reduction of Nitrate by Metallic Catalysts for High Efficiency and N2 Selectivity: A Review. *Chemical Engineering Journal* **2020**, *384*, No. 123252.
(61) Liu, Z.; Dong, S.; Zou, D.; Ding, J.; Yu, A.; Zhang, J.; Shan, C.; Gao, G.; Pan, B. Electrochemically Mediated Nitrate Reduction on Nanoconfined Zerovalent Iron: Properties and Mechanism. *Water Res.* **2020**, *173*, No. 115596.
(62) Jonoush, Z. A.; Rezaee, A.; Ghaffarinejad, A. Electrocatalytic Nitrate Reduction Using Fe0/Fe3O4 Nanoparticles Immobilized on Nickel Foam: Selectivity and Energy Consumption Studies. *Journal of Cleaner Production* **2020**, *242*, No. 118569.
(63) Chen, G.-F.; Yuan, Y.; Jiang, H.; Ren, S.-Y.; Ding, L.-X.; Ma, L.; Wu, T.; Lu, J.; Wang, H. Electrochemical Reduction of Nitrate to Ammonia via Direct Eight-Electron Transfer Using a Copper−Molecular Solid Catalyst. *Nat. Energy* **2020**, *5* (8), 605−613.
(64) Perry, S. C.; Gateman, S. M.; Stephens, L. I.; Lacasse, R.; Schulz, R.; Mauzeroll, J. Pourbaix Diagrams as a Simple Route to First Principles Corrosion Simulation. *J. Electrochem. Soc.* **2019**, *166* (11), C3186.
(65) Zuo, K.; Huang, X.; Liu, X.; Gil Garcia, E. M.; Kim, J.; Jain, A.; Chen, L.; Liang, P.; Zepeda, A.; Verduzco, R.; Lou, J.; Li, Q. A Hybrid Metal-Organic Framework-Reduced Graphene Oxide Nanomaterial for Selective Removal of Chromate from Water in an Electrochemical Process. *Environ. Sci. Technol.* **2020**, *54* (20), 13322−13332.

https://doi.org/10.1021/acsestengg.3c00507
ACS EST Engg. XXXX, XXX, XXX−XXX